ceramics

MDPI

Article

Recycling Face Mask Fibers in Geopolymer-Based Matrices for Sustainable Building Materials

Roberto Ercoli [1,*], Paola Stabile [1], Elena Ossoli [1], Irene Luconi [1], Alberto Renzulli [2] and Eleonora Paris [1]

[1] School of Science and Technology, Geology Division, University of Camerino, 62032 Camerino, Italy; paola.stabile@unicam.it (P.S.); elena.ossoli@unicam.it (E.O.); irene.luconi@unicam.it (I.L.); eleonora.paris@unicam.it (E.P.)

[2] Department of Pure and Applied Sciences, University of Urbino Carlo Bo, 61029 Urbino, Italy; alberto.renzulli@uniurb.it

* Correspondence: roberto.ercoli@unicam.it

Abstract: This study investigates the upcycling of disposable face masks, which were produced in vast quantities during the COVID-19 pandemic and are now widely stockpiled in public institutions, destined for landfills after reaching expiration dates. The research focuses on incorporating shredded mask fibers into geopolymer matrices, evaluating the effects on mechanical and thermal properties to develop sustainable, high-performance materials. This approach addresses critical environmental, social, and economic challenges by transforming problematic waste into valuable resources while promoting sustainable building practices, such as developing insulating products for the construction industry. Mechanical testing demonstrated that adding shredded mask fibers (2 mm and 6 mm in size, up to 5 wt.%) enhanced the flexural strength of geopolymeric products. The optimal performance was achieved by adding 3 wt.% of 2 mm-length fibers, resulting in a flexural strength of 4.56 ± 0.23 MPa. Regarding compressive strength, the highest value (54.78 ± 2.08 MPa) was recorded in geopolymers containing 1 wt.% of 2 mm fibers. Thermal insulation properties of the materials improved with higher mask content, as evidenced by reductions in thermal conductivity, diffusivity, and specific heat. The lowest thermal conductivity values were observed in geopolymers containing 5 wt.% (0.4346 ± 0.0043 $W \cdot m^{-1} \cdot K^{-1}$) and 3 wt.% (0.6514 ± 0.0002 $W \cdot m^{-1} \cdot K^{-1}$) of 2 mm mask fibers. To further enhance thermal insulation, geopolymers with 5 wt.% mask fibers were foamed using H_2O_2 to obtain highly porous light materials, obtaining a reduction of thermal conductivity (0.3456 and 0.3710 ± 0.0007 $W \cdot m^{-1} \cdot K^{-1}$). This research highlights the potential of integrating fibrous waste materials into advanced construction technologies, offering solutions for waste reduction and development in the building sector toward sustainability.

Keywords: face masks; geopolymers; upcycling; insulation

Academic Editors: Kinga Korniejenko and Aleksandar Nikolov

Received: 28 March 2025
Revised: 6 May 2025
Accepted: 7 May 2025
Published: 12 May 2025

Citation: Ercoli, R.; Stabile, P.; Ossoli, E.; Luconi, I.; Renzulli, A.; Paris, E. Recycling Face Mask Fibers in Geopolymer-Based Matrices for Sustainable Building Materials. *Ceramics* **2025**, *8*, 54. https://doi.org/10.3390/ceramics8020054

1. Introduction

The COVID-19 pandemic led to a dramatic increase in face masks, including surgical, FFP, N95, and cloth masks, as essential tools to prevent the spread of SARS-CoV-2. This surge in demand for personal protective equipment (PPE) also significantly increased medical waste generation. Masks were widely used in healthcare settings and by the public during daily activities, such as shopping and office work, contributing to an unprecedented volume of disposable mask waste.

This widespread use has created environmental challenges, as disposable masks are non-biodegradable and end up in landfills. Public institutions, schools, the army, industries,

and large private companies have stockpiled large quantities of masks for emergency preparedness. However, these stored masks face issues related to their limited shelf life and short expiration dates, leading to the need for periodic disposal of unused stock through landfilling. Therefore, the accumulation and disposal of such waste underscore the need for innovative solutions to manage this environmental burden. Upcycling or recycling initiatives that repurpose these materials into valuable products, such as construction or insulation, represent a promising solution for mitigating the environmental impact while addressing sustainability goals, like the EU directives for waste and landfill reduction [1] and the energy efficiency of buildings [2].

Face masks are primarily made from non-biodegradable polymers, such as melt-blown polypropylene (PP) and polyethylene (PE), both of which are petroleum-derived compounds that do not biodegrade [3]. It is worth noting that PE is the same polymer used in plastic shopping bags, which still represents a significant environmental concern, being a major unresolved issue contributing to global environmental pollution. The production of plastic, predominantly used for packaging and textiles, surged from 1.7 million metric tons in 1950 to 322 million metric tons in 2015. Consequently, it is estimated that approximately 8 million metric tons of plastic waste enters the oceans annually (~86% originating in the Asia Pacific region), adding to the roughly 250 million tons (equivalent to 5 trillion microplastic particles) already present on the ocean's surface [4].

For waste classification purposes, filter media materials are generally categorized as undifferentiated waste to be landfilled according to the procedures outlined in the COVID-19 Report (No. 3/2020) [5]. However, their extensive use has underscored the urgent environmental challenges associated with their widespread disposal, both controlled and uncontrolled, emphasizing the need to minimize landfilling [6]. Therefore, there is a growing imperative to explore new applications for this specific waste stream. Since masks are made of plastic fibrous materials, they can hold promise for successful upcycling, particularly for developing composite materials with diverse matrices [7]. However, it is crucial to adopt an approach that addresses identifying low-energy solutions and mitigating CO_2 emissions, contributing to climate change [8]. Consequently, any considerations involving chemical and thermal treatments (like incineration or pyrolysis) or the integration of mask waste into resin-based matrices (non-recyclable and destined for landfills) [9] or cementitious matrices (associated with high CO_2 emissions) should be reconsidered as not environmentally friendly.

In this regard, geopolymer-based products can offer a compelling alternative to cementitious binders [10]. The unique properties of geopolymers make them appealing for various applications in the construction, transportation, and industrial sectors. Key physical properties include (a) high-temperature resistance, rendering them suitable for extreme environments; (b) acid and corrosion resistance, making them applicable in harsh conditions; (c) high mechanical strength, ensuring the production of robust materials; (d) versatility, allowing for diverse forms and applications; (e) rapid setting for swift construction and repair; (f) low shrinkage to minimize cracking and enhance durability; (g) chemical stability, enabling use even in chemically aggressive environments [11].

Despite their many environmental and technical advantages, geopolymers' limitations hinder their widespread adoption. Their production requires complex processes and expensive materials, such as alkaline solutions. In addition, the polymerization process is sensitive to variations in the materials used, leading to inconsistent performance, and the supply of secondary raw materials used as precursors, such as fly ash and granulated blast furnace slag, is also increasingly limited due to environmental regulations. Thus, clear regulatory standards are lacking to ensure reliable performance over time [12]. However, geopolymers represent a promising solution for sustainability in the construction

sector, although further research is required to overcome their limitations and facilitate broader adoption.

Recycling within geopolymer matrices, therefore, entails an upcycling application for mask waste, diverting it from landfills or incineration to producing high-grade materials, like, for example, insulating panels for internal/external use. This approach offers environmental advantages over alternative recycling methods, such as room-temperature production without cement, allowing energy savings and low CO_2 emissions. Also, it presents economic benefits [13] by establishing a new green production paradigm through synergies among local industries, which can easily start as a viable prospect with the potential for replication anywhere.

The aim of this study is to evaluate the possibility of recycling disposable face masks through the incorporation of their fibers into geopolymer matrices and to analyze how this addition affects the mechanical and thermal properties of the resulting materials. In particular, the research aims to develop sustainable and high-performance construction materials, with a specific focus on obtaining insulating products for the building industry, thus offering a concrete solution both to the environmental problem of waste from masks and to the need for innovative materials for the construction sector.

2. Materials and Methods

Face masks work as mechanical barriers, obstructing direct airflow into and out of the respiratory openings, such as the nose and mouth, and are crucial in minimizing the airborne transmission of pathogens and other aerosolized particles between the mask wearer and those nearby. For these reasons, the design of masks varies depending on their intended use. Typically, the mask outer surface is thicker and water-resistant to enhance durability. The inner structure is composed of three layers of non-woven fabric (TNT), a thermoplastic material, usually polypropylene or polyester, that meets the functional requirements of the mask. Masks use two types of TNT: melt-blown and spun-bond. Spun-bond resembles a traditional fabric and is a non-woven polypropylene material. It is lightweight, breathable, and predominantly hydrophobic, making it ideal for blocking moisture in breath and protecting against blood spatter and other organic substances, including droplets. The melt-blown fabric, produced through a "blown spinning" technique, creates long, fine fibers that are cooled and collected onto a surface to form a delicate but effective filtering layer. This layer is crucial for the mask's ability to filter out particles, with its microfibers being less than 3 microns in size, directly impacting the mask's bacterial filtration efficiency (BFE) [14]. According to the European Standard EN 14683:2019 [15], Type I masks must achieve a BFE of 95%, while Type II and III masks must meet a BFE of 99%.

This study collected unused FFP2 face masks (Figure 1a–c) from a local school storage. The masks, including strings and nose holders, were shredded using a cutting mill with a rotor of six offset discs to prepare the material for further analysis. This process helped to break down the masks into smaller, more uniform fibers, making them easier to mix and work with. The shredded material was then sieved through 2 and 6 mm apertures, ensuring a consistent particle size before being collected.

The preliminary characterization of the masks was carried out using environmental scanning electron microscopy (ESEM) and Raman spectroscopy analyses (RAMAN) to check, respectively, for the composition, morphology, and molecular structure (Table 1).

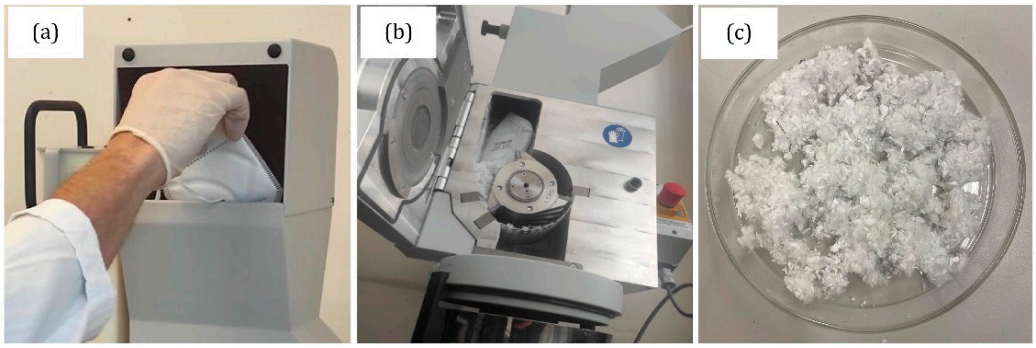

Figure 1. (**a**–**c**) Procedure for face mask shredding.

Physical properties, such as density, porosity, and mechanical and thermal properties, were measured to evaluate the effect of fiber size on the geopolymer matrix on the samples. All the instrumental and experimental details are reported in Table 1.

Table 1. Overview of instruments and experimental conditions.

Instruments	Model	Experimental Conditions
Mechanical Shredder	SM 300, Retsch GmbH, Haan, Germany	1500 rpm
Mechanical Mixer	60010020, Automix Controls, Milan, Italy	Following Norm EN 196-3:2017 [16], mixing time: 10 min
Environmental Scanning Electron Microscope (ESEM)	Ametek, Edax Inc., Mahwah, NJ, USA	kV: 25.00, Tilt: 0.00, Take-off: 35.00, AmpT: 51.2, Det Type: SUTW, Sapphire Res: 132.40, Lsec: 100
Raman Spectrometer (RAMAN)	iHR320, Horiba Scientific, Longjumeau, France	Acquisition time: 5 s, Accumulations: 10, Windows: 5, Objective: 100x, Laser: 532 nm
Pycnometer	Ultrapyc 5000, Anton Paar GmbH, Graz, Austria	Acquisition time: 10 sGas: Nitrogen
Porosimeter	PASCAL 240, Thermo Fisher Scientific Inc., Waltham, MA, USA	Pressure: 0.01–200 MPa Pore Size Range: 0.01–100 µm
Mechanical Tester	70-T2502, Controls, Milan, Italy	Following Norm EN 196-1:2016 [17]
Thermal Properties Tester	ISOMET 2114, Applied Precision Machines, Lake County, IL, USA	Following Norm ASTM C1363-19 [18]

2.1. Geopolymer Synthesis

The synthesis of geopolymers employed in this work used metakaolin, derived from the thermal treatment of kaolinite at temperatures ranging from 500 to 800 °C. During this process, structural hydroxyl ions were released. Subsequently, metakaolin underwent alkaline activation through the alkaline solution (potassium silicate). Mixing these two components resulted in the dissolution of Si-O and Al-O bonds, forming a supersaturated solution of the two groups. The material setting and the ensuing condensation (curing process) led to the aggregation and reorganization of the gel into polymers, consisting of

alternating silicon and aluminum tetrahedral structures at IV and IV–V coordination with oxygen, respectively [19].

The geopolymeric matrices were obtained using a commercial metakaolin (Metaver I, provided by Newchem, Milan, Italy) as the precursor and $K_2Si_2O_5$ (Reoflux A, provided by Ingessil Srl, Verona, Italy) as the activator (Table 2). The activation process was induced by mixing the two components for 8 min using a mechanical stirrer (Table 1). To optimize the material workability, we established experimental conditions with a $SiO_2/Al2O_3$ ratio of 1.97, a solid–liquid ratio of 0.9–1, and a pH value of 13.5 ± 0.5, as these parameters play a key role in determining its behavior (Table 2).

Table 2. Chemical and physical parameters of the starting materials for geopolymers and parameters set to produce geopolymer samples.

	Metaver I	**Reoflux A**
SiO_2 (wt.%)	53.5 ± 3.0	26.70 ± 2.10
Al_2O_3 (wt.%)	42.0 ± 2.0	–
Fe_2O_3 (wt.%)	<2.0	–
K_2O (wt.%)	<2.0	20.50 ± 0.60
Specific density ($kg \cdot m^{-3}$)	2600 ± 30	1410 ± 10
pH	–	13.5 ± 0.5
Ratios	**Values**	
n (SiO_2/Al_2O_3)	1.97	
n ($SiO_2/(Na_2O + K_2O)$)	3.38	
n ($Al_2O_3/(Na_2O + K_2O)$)	1.71	
Solid/Liquid ($kg \cdot L^{-1}$)	0.9–1.0	

Mask fibers were added to the geopolymer mix in 1, 3, and 5% by weight and mixed for 2 min to ensure homogenization. The quantities of inserted fiber masks corresponded to up to 8 whole masks for each kilogram of geopolymer sample produced. An extra geopolymer sample, consisting of metakaolin and $K_2Si_2O_5$ without mask fibers, was used for comparison. After the mixing, the geopolymer mortar was carefully poured into molds measuring 40 × 40 × 160 mm and 100 × 100 × 100 mm, designated for the three-point bending, compression tests, and thermal properties. The specimens were shielded with a polypropylene film and subjected to setting for approximately 24 h at room temperature (20 ± 2 °C). After the setting period, the samples were extracted from the molds, re-encased with a polypropylene film, and left at room temperature for 28 days for curing before performing any analysis.

After testing, the most performing geopolymer mixes were duplicated and foamed by adding 5 wt.% of H_2O_2 at the end of a 10 min mixing process to reduce density and enhance physical properties, which were also evaluated by the same experimental techniques.

2.2. Mechanical Testing

After 28 days of curing, the geopolymer specimens were tested using the three-point bending and compressive strength tests, which conformed to Standard UNI EN 196-1:2016 [17]. For each of the three-point bending tests, three specimens measuring 40 × 40 × 160 mm were tested at room temperature with a loading rate of 0.1 $MPa \cdot s^{-1}$ and a span length of 100 mm. The flexural strength (σ_f) was computed using Equation (1):

$$\sigma_f = 3L\frac{F_{max}}{2bh^2}(MPa), \quad (1)$$

where F_max is the maximum applied load indicated by the machine (N), L is the span length (mm), b is the width of the sample (mm), and h is the depth of the sample (mm).

Six segments (40 × 40 × 40 mm) from each sample type employed in the bending test were used for compressive strength (σ_c), which was determined using Equation (2):

$$\sigma_c = \frac{F_{max}}{A_c}(MPa), \quad (2)$$

where A_c is the cross-sectional area of the sample (mm^2).

2.3. Thermal Measurements

Thermal conductivity, thermal diffusivity, and specific heat were measured on a 100 × 100 × 100 mm sample (6 measurements on each face of the cube) using the instrument ISOMET 2114 and following the ASTM C1363-19 [18]. A known heat source generated a wave that propagated radially into the specimen. The dissipation of electrical energy produced heat flow through the probes in direct contact with the material, and an RS232C serial port recorded the signal. The temperature increased linearly with the logarithm of time. Semiconductor sensors at specific points on the materials recorded the temperature change over time.

Thermal conductivity (λ) was determined using Equation (3):

$$\lambda = \frac{Qd}{A\Delta T}\left(\frac{W}{mK}\right), \quad (3)$$

where Q is the amount of heat transferred, d is the distance between the two isotherms, A is the surface, and ΔT is the temperature gradient.

The specific heat capacity (C_p) is the heat needed to increase the temperature of 1 g of a substance by 1 °C and is given by Equation (4):

$$C_p = \frac{Q}{m\Delta T}\left(\frac{J}{kgK}\right), \quad (4)$$

where m is the mass.

The thermal diffusivity (α) quantifies the heat transfer rate of the material from the hot side to the cold side, and it was computed by Equation (5):

$$\alpha = \frac{\lambda}{\rho C_p}\left(\frac{mm^2}{sec}\right), \quad (5)$$

where ρ is the density of the geopolymer.

3. Results

3.1. Characterization of Starting Materials

Back-scattered electron (BSE) analyses of FFP2 masks (Figure 2) revealed a complex fibrous structure, with fibers ranging from 10 to 20 μm in diameter. The main morphological differences between mask fragments of 2 and 6 mm are shown in Figure 2a,d, respectively.

The 2 mm fibers appeared more compact and homogeneously distributed, forming a dense and entangled fibrous network (Figure 2a). In contrast, the 6 mm fragments exhibited a looser and less uniform structure, with more pronounced voids and less interconnection between fibers (Figure 2d). In both types, some more prominent and elongated fibers corresponding to fragments of nose holders (Figure 2b,c) and elastic bands (Figure 2f) were included to consider the need to avoid component separation in the possible recycling process.

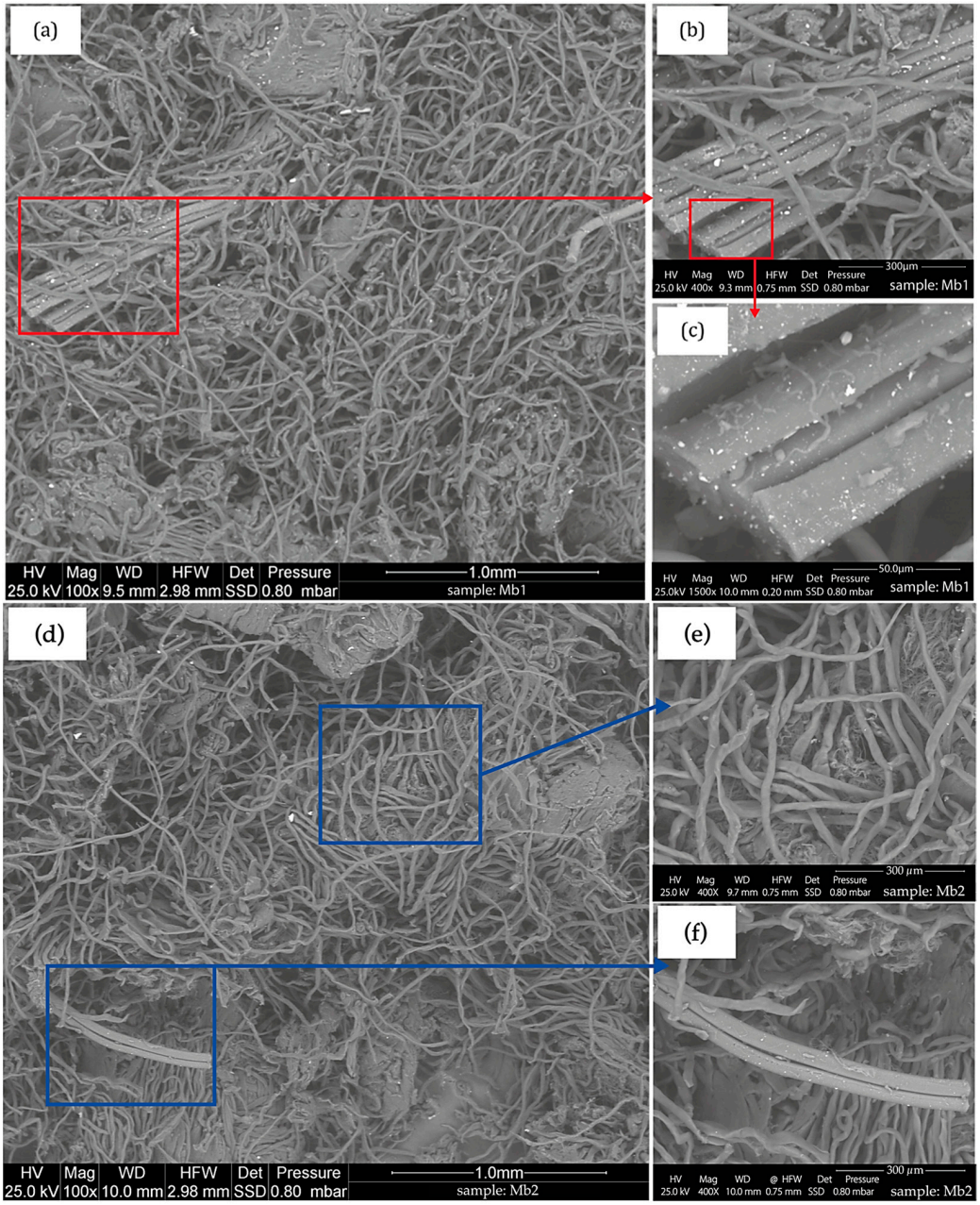

Figure 2. (**a**). Fibrous structure (2 mm in length) of the shredded FFP2 mask layers, evenly distributed to form a dense network. The shredded nose band (highlighted with a red square) is magnified in (**b**) at 400× and in (**c**) at 1500×. (**d**) Low-magnification image of fibers shredded to 6 mm in length, (**e**) magnified at 400×, and (**f**) showing a fragment of the elastic ear loops (corresponding areas in blue squares).

Raman spectra have been acquired on the masks to determine their composition, and the results are reported in Figure 3. Focusing on the high-wavenumber (HW, 750–1250 cm^{-1}) region of the Raman spectra, the most relevant peaks were centered at around 400 cm^{-1}, 800 cm^{-1}, 1150 cm^{-1}, 1300 cm^{-1}, and 1450 cm^{-1}, and peak positions were characteristic of polymeric materials, such as polyethylene (PE) and polypropylene (PP). The peaks around 850 cm^{-1} and 1046 cm^{-1} were associated with the vibrational modes of C–C and C–H bonds in the polymer backbone. Due to its distinct molecular structure, these peaks were generally more intense in PE. On the other hand, the peaks at 1300 cm^{-1} and 1450 cm^{-1} corresponded to CH_2 bending vibrations observed in both PE and PP. The difference among the spectra related to the three mask layers resided in the

peak intensity and, in turn, the relevance of one polymer phase rather than the other in each layer. However, this aspect was not considered since the waste is considered bulk, making it impossible to separate each layer before shredding.

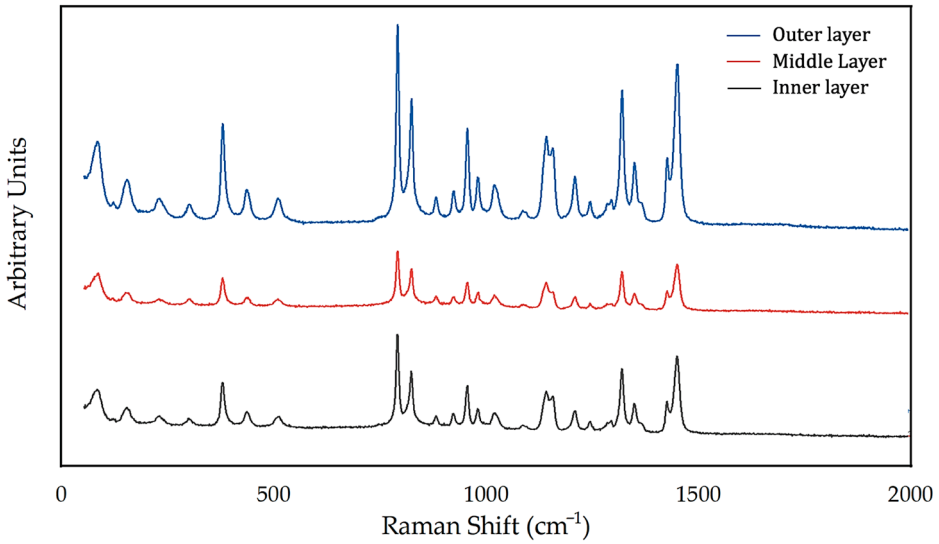

Figure 3. Raman spectra of the three layers of the FFP2 face masks.

3.2. Geopolymer Samples

Six geopolymer specimens were produced with a variable amount of FFP2 mask (1, 3, and 5 wt.%) and different fiber sizes (2 and 6 mm). A macro-photograph of one example of geopolymer (specimen GP.Mb1_5%) is reported in Figure 4a, while Figure 4b shows the dispersion of fibers throughout the different samples. Six geopolymer specimens were produced with a variable amount of FFP2 mask (1, 3, and 5 wt.%) and different fiber sizes (2 and 6 mm).

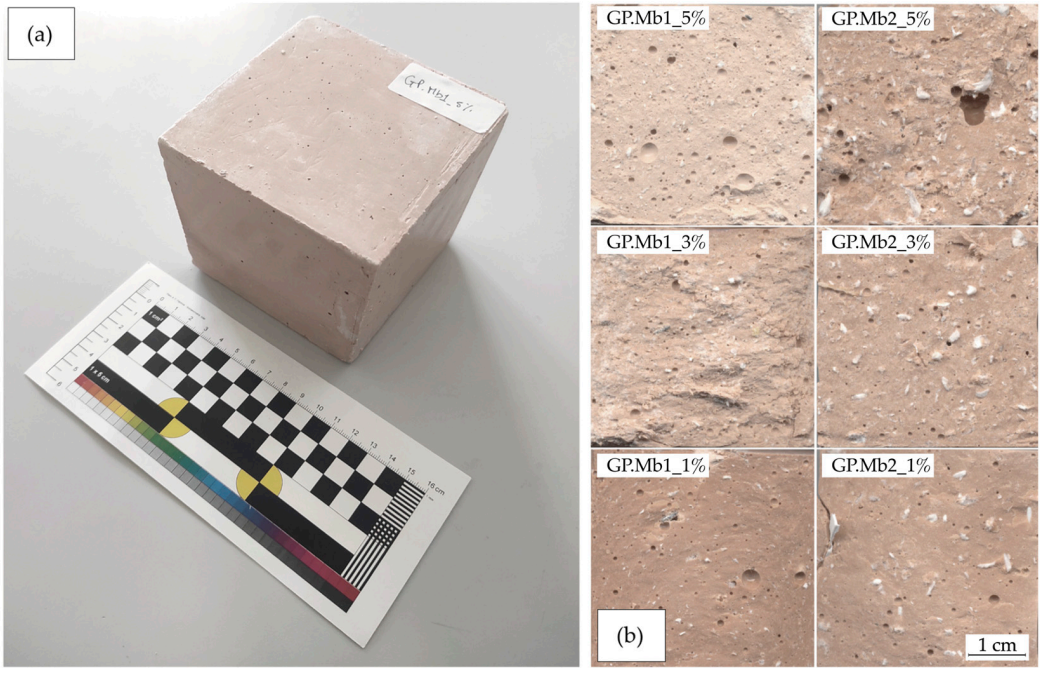

Figure 4. (**a**) GP.Mb1_5% produced for testing thermal properties. (**b**) Surface sections of all the samples incorporating different mask fiber amounts (1, 3, and 5 wt.%) and varying sizes (2 or 6 mm).

The data summarized in Table 3 demonstrate the influence of mask fiber incorporation on the physical, mechanical, and thermal properties of geopolymer samples. Adding increasing quantities of mask fibers to the samples reduced their density due to their lightweight nature, creating voids and enhancing the porosity of the geopolymer matrix. Adding 5 wt.% of fibers reduced the density by 9.58 ± 1.08% between the reference sample (GP.STD.b) and the sample GP.Mb2_5%, with a further decrease obtained for foamed geopolymers (as detailed in Section 3.3).

Table 3. Physical and mechanical properties of the geopolymers.

	Geopolymer Sample (GP.)								
Parameter	**STD.b**	**Mb1_1%**	**Mb2_1%**	**Mb1_3%**	**Mb2_3%**	**Mb1_5%**	**Mb2_5%**	**Mb1_5%-f**	**Mb2_5%-f**
Mask content m_f (wt.%)	0	1	1	3	3	5	5	5	5
Fiber length l (mm)	0	2	6	2	6	2	6	2	6
Density ρ (kg·m^{-3})	1777.50 ± 14.83	1686.81 ± 17.71	1682.59 ± 15.18	1639.91 ± 27.45	1680.37 ± 22.65	1579.05 ± 3.20	1607.19 ± 13.73	580.39 ± 20.13	600.83 ± 21.20
Porosity φ (%)	21.6	27.5	26.6	32.3	31.7	35.8	34.4	53.0	50.9
Compressive strength σc (MPa)	52.42 ± 3.06	54.78 ± 2.08	52.49 ± 3.69	48.71 ± 2.43	47.34 ± 1.38	41.96 ± 4.29	39.46 ± 2.06	3.30 ± 0.37	4.80 ± 0.56
Flexural strength σf (MPa)	3.23 ± 0.38	3.77 ± 0.14	3.49 ± 0.34	4.56 ± 0.23	3.78 ± 0.46	4.00 ± 0.21	4.20 ± 0.36	1.58 ± 0.34	1.79 ± 0.06
Thermal conductivity λ (W·m^{-1}·K^{-1})	0.7658 ± 0.0082	0.6951 ± 0.0010	0.7342 ± 0.0063	0.6592 ± 0.0056	0.6514 ± 0.0002	0.4346 ± 0.0043	0.6125 ± 0.0057	0.3456 ± 0.0007	0.3710 ± 0.0007
Specific heat C_p (J·kg^{-1}·K^{-1})	0.4714 ± 0.0047	0.4046 ± 0.0005	0.4403 ± 0.0035	0.3919 ± 0.0019	0.4167 ± 0.0003	0.2681 ± 0.0026	0.3941 ± 0.0037	0.2235 ± 0.0007	0.2512 ± 0.0004
Thermal diffusivity α (m^2·s^{-1})	1.6245 ± 0.0024	1.7178 ± 0.0036	1.6677 ± 0.0022	1.6822 ± 0.0061	1.5632 ± 0.0008	1.6211 ± 0.0009	1.5542 ± 0.0005	1.5463 ± 0.0035	1.4768 ± 0.0001

3.2.1. Mechanical Properties

The results obtained for the compressive strength (Table 3 and Figure 5a) demonstrated that incorporating mask fibers into geopolymer matrices allowed for reaching excellent compressive strength values and maintaining high values for all samples. When adding a 1 wt.% mask, these were even higher than the values of the reference sample. Even if there was an expected decrease in compressive strength at the higher quantities of fibers added (5 wt.%), the values obtained still ranged approximately between 40 and 55 MPa.

In particular, the highest compressive strength values were observed in samples with 1 wt.% mask fibers, specifically GP.Mb1_1%: 54.78 ± 2.08 MPa, and GP.Mb2_1%: 52.49 ± 3.69 MPa. These results indicate that smaller fiber contents (1 wt.%) optimized the reinforcement effect of the mask fibers within the geopolymer matrix. However, as the mask content and fiber size increased, a gradual reduction in compressive strength could be observed. For instance, the sample with 5 wt.% of 6 mm fibers (GP.Mb2_5%) exhibited the lowest compressive strength of 39.46 ± 2.06 MPa. These findings suggest that while low mask contents enhanced mechanical properties, on the other hand, the excessive fiber content or larger fiber sizes may weaken the matrix–fiber interaction and introduce defects, thus reducing the compressive strength. Nonetheless, even with higher fiber content, the

excellent structural performance makes these mortars viable for high-grade construction applications (Figure 5a).

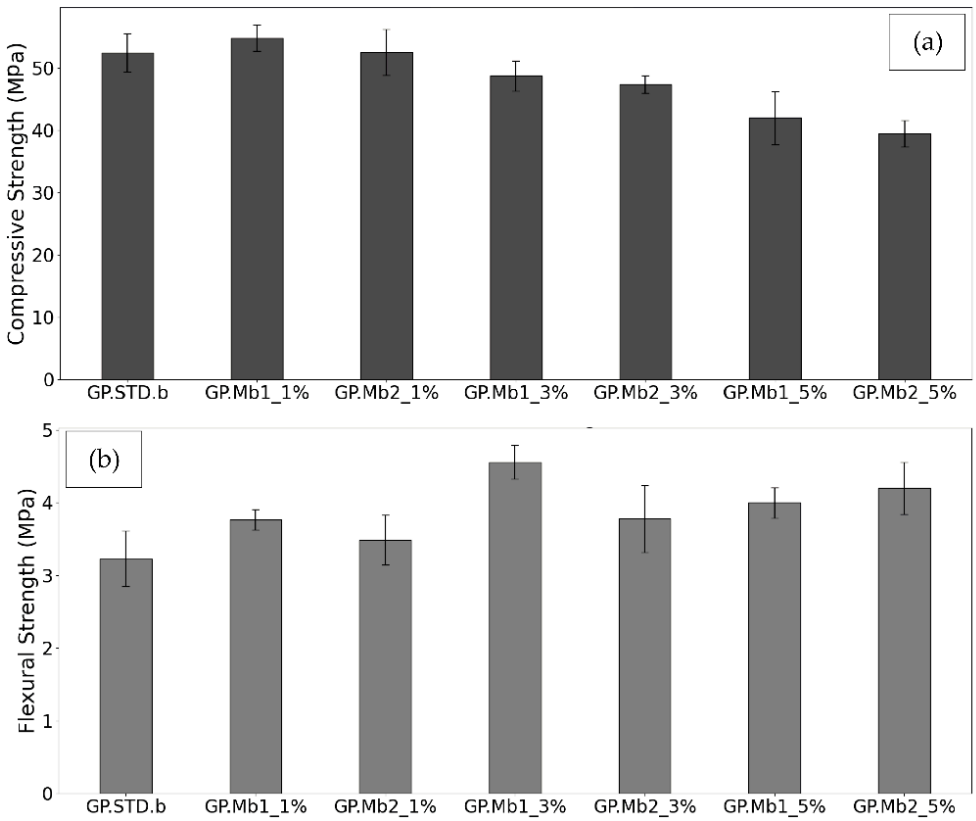

Figure 5. (**a**) Compressive and (**b**) flexural strengths of the six geopolymers with different mask contents, compared to the Standard GP.STD.b, which does not contain mask fibers.

On the other hand, adding mask fibers significantly enhanced the flexural strength of the geopolymer samples compared to the standard sample (GP.STD.b) produced without fibers (Table 3 and Figure 5b). Flexural strength generally increased with higher fiber content, ranging from 1 wt.% to 5 wt.%, with the best performance observed for the GP.Mb1_3% sample with a flexural strength of 4.56 $\pm$ 0.23 MPa. The results also indicated that the composite with 6 mm fibers exhibited lower flexural strength than those with 2 mm fibers across all tested concentrations (Table 3 and Figure 5b). This behavior of longer fibers arose from three synergistic factors: (1) agglomeration during mixing, which created localized weak zones, (2) increased interfacial porosity due to poor fiber–matrix packing, and (3) the critical length for effective stress transfer.

Figure 6a further illustrates the extent to which mask fibers influenced the mechanical behavior of the geopolymers over the testing time. The presence of mask fibers delayed the onset of fracturing and provided additional post-fracture resistance, as evidenced by secondary peaks in the flexural strength curves. While the reference sample (GP.STB.b) broke sharply after 27 s from the start of the test, the samples containing fibers gained up to 10.5 s before breaking (e.g., GP.Mb1_3%), with an increase of around 28%. This behavior highlights the ability of mask fibers to bridge cracks (Figure 6b,c) and sustain loads even after initial failure, contributing to improved mechanical resistance.

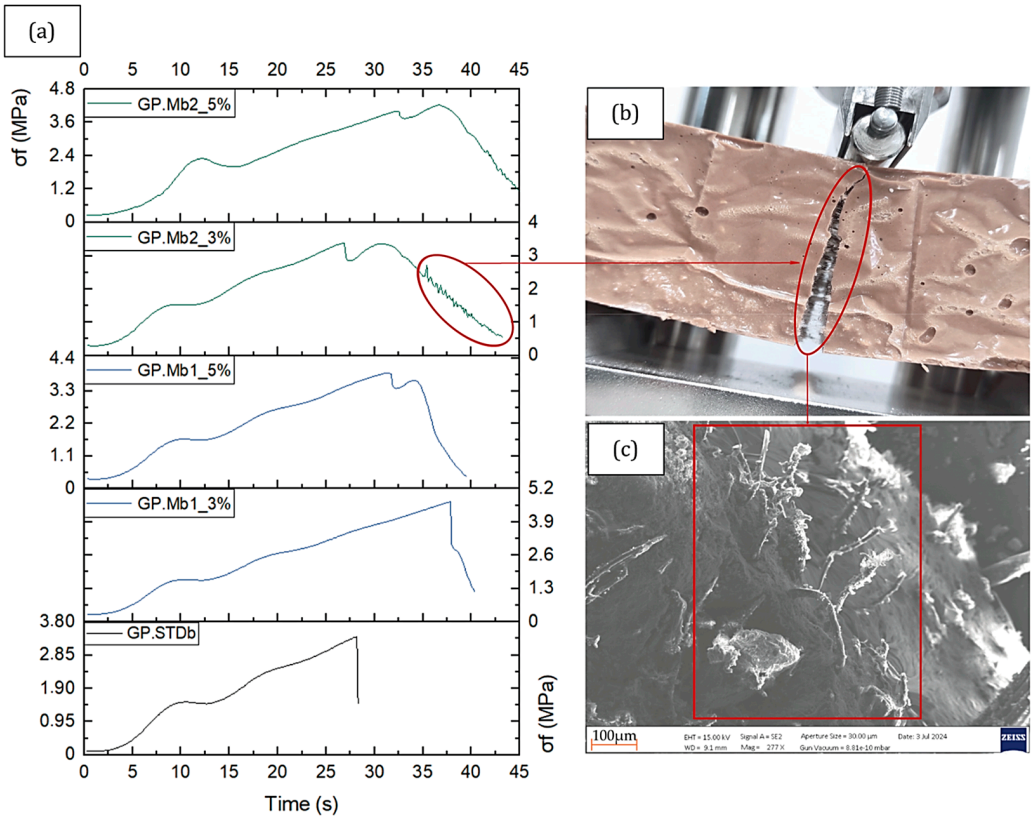

Figure 6. (**a**) Influence of mask content on crack formation delay and the post-rupture fiber bridging effect during the flexural test, (**b**,**c**) Optical and ESEM images showing the strain of fibers on the fracture surface of sample GP.Mb2_3%.

3.2.2. Thermal Properties

The thermal properties measured in this study, i.e., thermal conductivity, thermal diffusivity, and specific heat (Table 3 and Figure 7), offer valuable insights into the material thermal behavior, including its ability to conduct heat, respond to temperature changes, and store heat energy.

Focusing on thermal conductivity (λ), the standard geopolymer sample (GP.STD.b) exhibited 0.7658 ± 0.0082 $W \cdot m^{-1} \cdot K^{-1}$. In contrast, samples containing mask fibers demonstrated significantly lower thermal conductivity values, highlighting the adequate insulating capacity due to the added fibers. Among all the tested samples, the GP.Mb1_5% sample (containing 5 wt.% of 2 mm fibers) achieved the lowest thermal conductivity value of 0.4346 ± 0.0043 $W \cdot m^{-1} \cdot K^{-1}$. This represents a substantial reduction of 43.24% in thermal conductivity compared to the standard sample.

The thermal diffusivity (α) results showed only minor fluctuations with the addition of mask fibers, indicating that the rate of heat spread within the geopolymer matrix remained largely unaffected. For example, the control sample (GP.STD.b) exhibited a thermal diffusivity of 1.6245 ± 0.0024 $m^2 \cdot s^{-1}$, while the GP.Mb1_5% sample (containing 5 wt.% of 2 mm fibers) showed a slightly lower value of 1.6211 ± 0.0009 $m^2 \cdot s^{-1}$ (Figure 7).

In contrast, adding mask fibers generally led to a noticeable decrease in specific heat (C_p) values. For instance, the standard sample had a specific heat of 0.4714 ± 0.0047 $J \cdot kg^{-1} \cdot K^{-1}$, whereas the GP.Mb1_5% sample exhibited a significantly lower specific heat of 0.2681 ± 0.0026 $J \cdot kg^{-1} \cdot K^{-1}$.

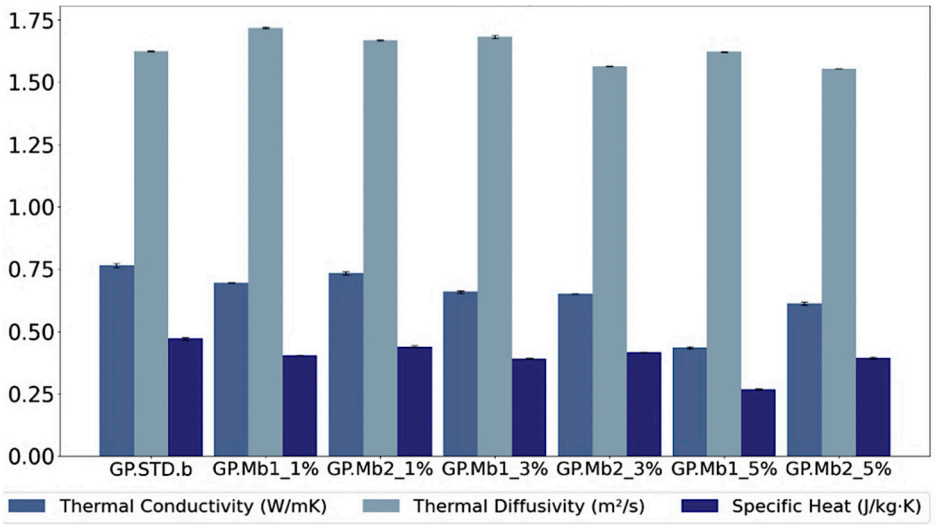

Figure 7. Thermal conductivity, thermal diffusivity, and specific heat are functions of the mask content and fiber size.

3.3. Foamed Geopolymers

Samples containing the highest mask fiber content (5 wt.%) were selected and further modified through a foaming process using 5 wt.% of hydrogen peroxide (H_2O_2) to enhance the properties of the geopolymers for possible applications in the construction sector as lightweight. As expected, the foamed samples had significantly lower mechanical properties than their non-foamed counterparts (Table 3) because of their higher porosity. The samples displayed porosity values of 53% and 50.9%, respectively (Table 3), to be compared to 35.8% and 34.4% values measured for the non-foamed ones. The foaming process resulted in samples characterized by a highly porous structure (Figure 8a) and a peculiar distribution of pore volumes (Figure 8b).

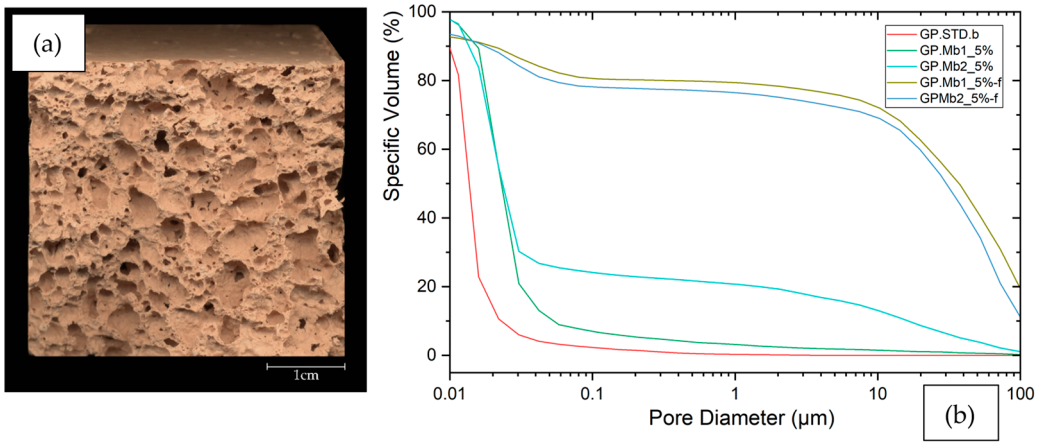

Figure 8. (**a**) Foamed geopolymer (GP-Mb2_5%-f; 40 × 40 mm section) and (**b**) specific volume as a function of pore diameter (0.01–100 μm) of the standard, the samples with >5% mask, and foams.

The foamed samples (GP.Mb1_5%-f and GP.Mb2_5%-f) exhibited pore size distributions (measured between 0.01 and 100 μm) much broader than those of the other samples and the standard, as shown in Figure 8b. These formulations showed, therefore, an increased presence of larger pores, higher overall specific volume porosity, and an expanded range of pore sizes. These increased values, around 1.5 times for both samples, also correlated with the substantial decrease in density and thermal conductivity

observed in the foamed samples, highlighting the trade-off between mechanical strength and thermal insulation.

The foamed samples exhibited significant improvements in thermal insulation (Table 3): thermal conductivity was reduced by 20.50 ± 0.80% for GP.Mb1_5%-f and even −39.43 ± 0.58% for GP.Mb2_5%-f. In addition to thermal conductivity, the thermal diffusivity and specific heat capacity reductions provided further insights into the material's behavior. The decrease in thermal diffusivity (−4.61 ± 0.22% for GP.Mb1_5%-f and −4.98·0.03% for GP.Mb2_5%-f) indicated that the material slowed down the rate at which heat propagated through it, which is advantageous for maintaining stable temperatures to favor insulated environments.

Additionally, the reduction of specific heat capacity (−16.64 ± 0.85% for GP.Mb1_5%-f and −36.26 ± 0.61% for GP.Mb2_5%-f) suggested that the material required less energy to promote temperature changes. This could benefit applications requiring a rapid thermal response or minimal heat storage. This strong reduction in thermal properties demonstrated the effectiveness of the foaming process in producing an increased porosity, which is useful for obtaining a lightweight material with reduced density and is designed to be used as a non-structural insulating panel [20,21].

4. Discussion

Thermal properties are essential in evaluating the suitability of materials for applications where insulation and energy efficiency are critical. The study results revealed a good correlation (R = 0.86) between the physical and thermal properties of the samples presented in this study (Figure 9). Density values decreased with increased mask fibers, from 1777.50 ± 14.83 kg·m^{-3} in the standard sample (GP.STD.b) to 1579.05 ± 3.20 kg·m^{-3} in the 5 wt.% sample (GP.Mb1_5%). It is important to note that density decreased to 580.39 ± 20.13 kg·m^{-3} for the foamed counterpart sample (GP.Mb1_5%-f), with a total decrease of 67.35 ± 1.16%. This suggested that the materials developed in this study were considerably light (<1400 kg·m^{-3}) [22] and could offer advantages for applications requiring reduced weight and improved insulation properties compared to other products.

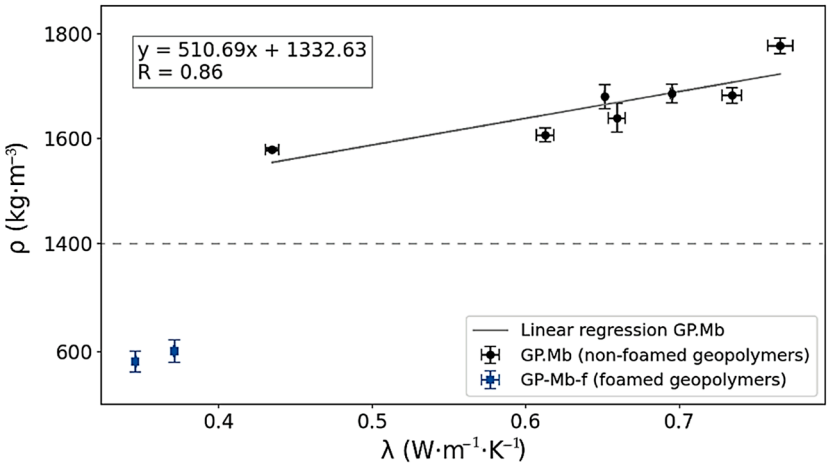

Figure 9. Correlation between density and thermal conductivity for the non-foamed geopolymers (top). The foamed samples are shown at the bottom of the plot, evidencing reduced density and thermal conductivity values.

Considering the non-foamed samples, the reduction in thermal conductivity can be attributed to the progressively higher mask fiber content. However, it is evident that at the highest quantities of mask fibers added, smaller fibers (2 mm) played a different role than 6 mm fibers, contributing even more to effectively disrupting heat transfer pathways

within the geopolymer matrix and promoting insulation. Moreover, the foaming process of the geopolymer samples helped to change thermal properties by strongly producing additional porosity in the samples, further reducing density and thermal conductivity.

A comparative analysis of the thermal conductivity measured in these samples against standard construction and insulation materials [23–26] and similar materials produced in [27] is shown in Figure 10. When compared to common insulating materials, such as polystyrene (0.18 ± 0.01 W·m^{-1}·K^{-1}) [23] and rock wool (0.035 ± 0.005 W·m^{-1}·K^{-1}) [24], the foamed geopolymers approached competitive thermal insulation performance, while offering a sustainable alternative through waste valorization. Moreover, even if the geopolymers containing mask fibers did not achieve the extremely low thermal conductivity characteristic of the rock wool, they offered a substantial improvement over standard concretes (with thermal conductivity of 2.69 ± 0.18 W·m^{-1}·K^{-1}) [25] and bricks (0.8 ± 0.1 W·m^{-1}·K^{-1}) [26].

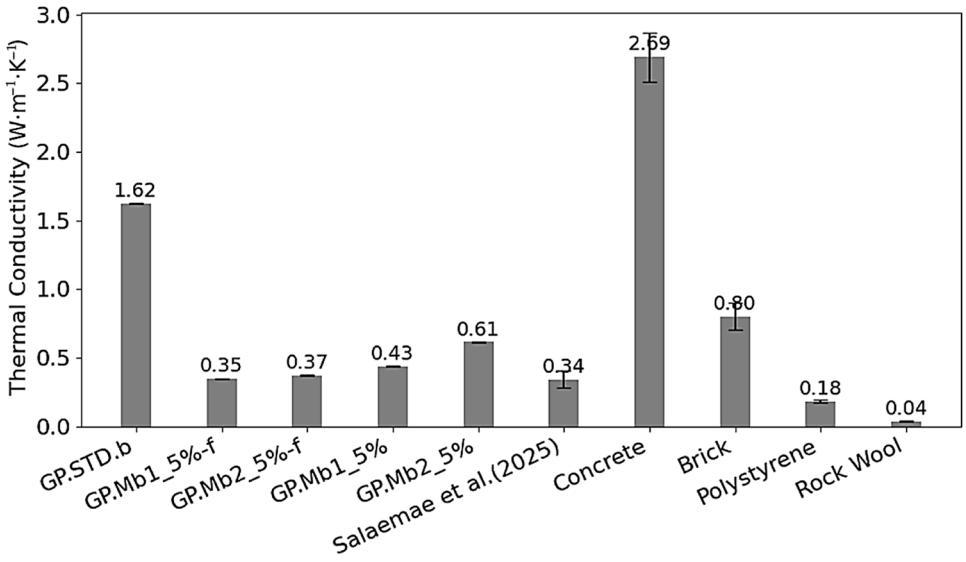

Figure 10. Thermal conductivity of the reference sample and geopolymers with 5 wt.% mask fibers (both foamed and non-foamed samples) compared to geopolymer mortars incorporating palm oil clinker (POC) and mask fragments as aggregates, from Salaemae et al., 2025 [27], standard concrete and bricks without fibers, as well as conventional insulating materials, such as polystyrene and rock wool [23–26].

The thermal conductivity of foamed geopolymers was comparable to that of geopolymer mortars containing 2–6 wt.% face mask fragments, as reported by Salaemae et al., 2025 [27], which exhibited an average thermal conductivity of 0.34 ± 0.0614 W·m^{-1}·K^{-1}. These values were obtained on samples produced using fly ash as a precursor, activated with an alkali solution, and palm oil clinker (POC) as an aggregate. Thus, although those authors used precursors and activators different from those we introduced in our samples, their results support the effectiveness of incorporating face mask waste in reducing thermal conductivity across different experimental setups and geopolymer components.

Few other studies also focused on producing geopolymer bricks containing face mask fragments (Salaemae et al., 2025; Thoudam et al., 2023; Win et al., 2023) [27–29]. For instance, Thoudam et al., 2023 [28] examined bricks made with alkali-activated binders, including ground-granulated blast furnace slag (GGBS) and rice husk ash (RHA), with recycled surgical masks. Their mechanical strength results were much lower than those obtained for our samples and compared well only with our foamed counterparts and with the results by Salaemae et al., 2025 [27] (Figure 11). Win et al., 2023 [29] focused instead on the cement

mortars reinforced with polypropylene fibers derived from surgical masks. Despite the cement binders used, our samples compared well to them in terms of compressive strength.

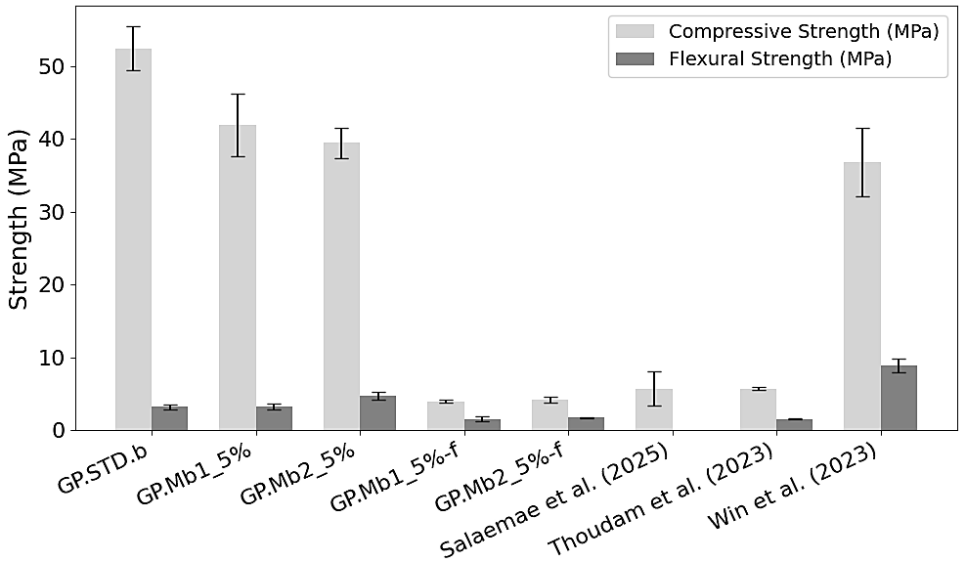

Figure 11. Comparisons of compressive and flexural strength (MPa) of our samples compared to some literature data [27–29].

Finally, the findings we reported in the present study are consistent with research on fiber-reinforced geopolymer composites by Ranjbar et al., 2016 [30]. However, unlike the industrial polypropylene fibers, the mask fibers used here offered comparable improvements in flexural strength, particularly at optimal fiber contents (3 wt.% in both cases) and optimal thermal properties, while addressing critical environmental concerns related to waste management and introducing a sustainable approach.

5. Conclusions

This study demonstrated that incorporating shredded face mask fibers into geopolymer matrices effectively enhanced both mechanical and thermal properties.

The addition of mask fibers (particularly 2 mm in length) led to a marked increase in flexural strength, with the best result (4.56 ± 0.23 MPa) achieved at 3 wt.% fiber content. Compressive strength peaked at 54.78 ± 2.08 MPa with 1 wt.% of 2 mm fibers, indicating that small amounts of fibers can reinforce the matrix without compromising its integrity. Thermal properties improved significantly as the mask fiber content increased. The lowest thermal conductivity (0.4346 ± 0.0043 $W \cdot m^{-1} \cdot K^{-1}$) was recorded in geopolymers containing 5 wt.% of 2 mm fibers. Further improvements were achieved by foaming the geopolymer with H_2O_2, reducing density by up to 67% compared to the standard and lowering thermal conductivity to values of 0.3456 ± 0.0007 $W \cdot m^{-1} \cdot K^{-1}$.

Overall, these results confirmed that upcycling face mask waste in geopolymers not only diverted non-biodegradable materials from landfills but also yielded lightweight, high-performance building materials suitable for insulation applications. This approach offers a practical step toward sustainable construction and circular economy goals by transforming problematic waste into valuable resources.

Author Contributions: Conceptualization, E.P., R.E., E.O. and P.S.; formal analysis, R.E. and E.P.; funding acquisition, E.P.; investigation, R.E.; methodology, R.E.; project administration, E.P. and R.E.; resources, E.P.; supervision, R.E. and E.P.; validation E.P., R.E., A.R. and P.S.; visualization, E.P., R.E., A.R., P.S. and I.L.; writing—original draft, R.E.; writing—review and editing, R.E., P.S. and E.P. All authors have read and agreed to the published version of the manuscript.

Funding: This research was funded by Fondazione TIM (TIM-Maskverde project, STI 512004) to E.P. P.S. acknowledges funding from Progetto Coesione (TRAILEDLAB, CUP E97G23000250001). R.E. acknowledges funding from the MUR-PRIN 2022 Project RUB2RES.

Institutional Review Board Statement: Not applicable.

Informed Consent Statement: Not applicable.

Data Availability Statement: Data is contained within the article.

Conflicts of Interest: The authors declare no conflicts of interest.

References

1. European Parliament. Directive (EU) 2018/850 of the European Parliament and of the Council, of 30 May 2018, amending Directive 1999/31/EC on the landfill of waste. *Off. J. Eur. Union L* **2018**, *150*, 100–108.
2. European Parliament. Directive (EU) 2018/844 of the European Parliament and of the Council, of 30 May 2018, amending Directive 2010/31/EU on the energy performance of buildings and Directive 2012/27/EU on energy efficiency. *Off. J. Eur. Union L* **2018**, *156*, 75–91.
3. Kan, C.-W.; Zille, A.; Rahman, M.Z.; Hoque, M.E.; Alam, M.R.; Rouf, M.A.; Islam Khan, S.; Xu, H.; Ramakrishna, S. Face Masks to Combat Coronavirus (COVID-19)—Processing, Roles, Requirements, Efficacy, Risk and Sustainability. *Polymers* **2022**, *14*, 1296. [CrossRef]
4. Geyer, R.; Jambeck, J.R.; Law, K.L. Production, use, and fate of all plastics ever made. *Sci. Adv.* **2017**, *3*, e1700782. [CrossRef] [PubMed]
5. World Health Organization (WHO). *Novel Coronavirus (2019-nCoV) Situation Report*; COVID-19 Report No. 3/2020; WHO: Geneva, Switzerland, 2024; Available online: https://iris.who.int/handle/10665/330762 (accessed on 20 March 2025).
6. Ajaj, R.; Al Dweik, R.; Ali, S.A.S.; Stietiya, M.H. Understanding the environmental impacts of facemasks: A review on the facemask industry and existing life cycle assessment studies. *Sustain. Environ. Res.* **2023**, *33*, 20. [CrossRef]
7. Maloba, J.W.; Kiambigi, J.M.; Kabubo, C.K. Reutilizing Single-Use Surgical Face Masks to Improve the Mechanical Properties of Concrete: A Feasibility Study. *Eng. Technol. Appl. Sci. Res.* **2023**, *13*, 10511–10516. [CrossRef]
8. United States Environmental Protection Agency (EPA). National Recycling Strategy: Building a Circular Economy for All. 2024. Available online: https://www.epa.gov/sites/default/files/2020-10/documents/draft_national_recycling_strategy.pdf (accessed on 20 March 2025).
9. Saitta, L.; Rizzo, G.; Tosto, C.; Cicala, G.; Blanco, I.; Pergolizzi, E.; Ciobanu, R.; Recca, G. Chemical Recycling of Fully Recyclable Bio-Epoxy Matrices and Reuse Strategies: A Cradle-to-Cradle Approach. *Polymers* **2023**, *15*, 2809. [CrossRef]
10. Furtos, G.; Prodan, D.; Sarosi, C.; Moldovan, M.; Korniejenko, K.; Miller, L.; Fiala, L.; Novakova, I. Mechanical Properties of MiniBars Basalt Fiber-Reinforced Geopolymer Composites. *Materials* **2024**, *17*, 248. [CrossRef] [PubMed]
11. Andrew, R.M. Global CO_2 emissions from cement production, 1928–2018. *Earth Syst. Sci. Data* **2018**, *10*, 221–236. [CrossRef]
12. Jabar, T.; Abed, M.; Alzuhairi, M.A. A comprehensive review on geopolymer materials: Preparation, properties, applications, and challenges. In Proceedings of the 4th International Conference on Innovation in IoT, Robotics and Automation (IIRA 4.0), Moradabad, India, 15–16 March 2024. [CrossRef]
13. Muda, I.; Dias, R.; Chetthamrongchai, P.; Jalil, A.T. An Environmentally Friendly Solution for Waste Facial Masks Recycled in Construction Materials. *Sustainability* **2022**, *14*, 8739. [CrossRef]
14. Oberg, T.; Brosseau, L.M. Surgical mask filter and fit performance. *Am. J. Infect. Control* **2008**, *36*, 276–282. [CrossRef] [PubMed]
15. *EN 14683:2019+AC:2019*; Medical Face Masks—Requirements and Test Methods. European Committee for Standardization (CEN): Brussels, Belgium, 2019.
16. *UNI EN 196-3:2017*; Metodi di Prova per Cementi—Parte 3: Determinazione del Tempo di Presa e della Stabilità di Volume. Ente Nazionale Italiano di Unificazione (UNI): Milano, Italy, 2017.
17. *UNI EN 196-1:2016*; Metodi di Prova per Cementi—Parte 1: Determinazione della Resistenza a Compressione. Ente Nazionale Italiano di Unificazione (UNI): Milano, Italy, 2016.
18. *ASTM C1363-19*; Standard Test Method for Thermal Performance of Building Materials and Envelope Assemblies by Means of a Hot Box Apparatus. ASTM International: West Conshohocken, PA, USA, 2019.
19. Biel, O.; Rożek, P.; Florek, P.; Mozgawa, W.; Król, M. Alkaline Activation of Kaolin Group Minerals. *Crystals* **2020**, *10*, 268. [CrossRef]
20. Ercoli, R.; Laskowska, D.; Nguyen, V.V.; Le, V.S.; Louda, P.; Łoś, P.; Ciemnicka, J.; Prałat, K.; Renzulli, A.; Paris, E.; et al. Mechanical and Thermal Properties of Geopolymer Foams (GFs) Doped with By-Products of the Secondary Aluminum Industry. *Polymers* **2022**, *14*, 703. [CrossRef] [PubMed]

21. Nguyen, V.V.; Le, V.S.; Louda, P.; Szczypiński, M.M.; Ercoli, R.; Růžek, V.; Łoś, P.; Prałat, K.; Plaskota, P.; Pacyniak, T.; et al. Low-Density Geopolymer Composites for the Construction Industry. *Polymers* **2022**, *14*, 304. [CrossRef]
22. Ossoli, E.; Volpintesta, F.; Stabile, P.; Reggiani, A.; Santulli, C.; Paris, E. Upcycling of composite materials waste into geopolymer-based mortars for applications in the building sector. *Mater. Lett.* **2022**, *333*, 133625. [CrossRef]
23. Kharun, M.; Svintsov, A.P. Polystyrene concrete as the structural thermal insulating material. *Int. J. Adv. Appl. Sci.* **2017**, *4*, 40–45. [CrossRef]
24. Ablaoui, E.M.; Malendowski, M.; Szymkuc, W.; Pozorski, Z. Determination of Thermal Properties of Mineral Wool Required for the Safety Analysis of Sandwich Panels Subjected to Fire Loads. *Materials* **2023**, *16*, 5852. [CrossRef]
25. Pagola, M.A.; Jensen, R.L.; Madsen, S.; Poulsen, S.E. *Measurement of Thermal Properties of Soil and Concrete Samples*; DCE Technical Reports, No. 235; Aalborg University, Department of Civil Engineering: Aalborg, Denmark, 2017.
26. Khomenko, O.S.; Sribniak, N.; Ivchenko, V.; Ujma, A.; Pomada, M. Thermal conductivity study of different engobed ceramic bricks. *Cerâmica* **2024**, *70*, 6–102. [CrossRef]
27. Salaemae, P.; Abdulmatin, A.; Prachasaree, W.; Hawa, A. Enhancing geopolymer mortars: The role of surgical face masks in modifying mechanical and thermal properties. *Eng. Appl. Sci. Res.* **2025**, *52*, 1–6. [CrossRef]
28. Thoudam, K.; Hossiney, N.; Kumar, S.L.; Alex, J. Recycled surgical mask waste as a resource material in sustainable geopolymer bricks. *Recycling* **2023**, *8*, 93. [CrossRef]
29. Win, T.T.; Jongvivatsakul, P.; Jirawattanasomkul, T.; Prasittisopin, L.; Likitlersuang, S. Use of polypropylene fibers extracted from recycled surgical face masks in cement mortar. *Constr. Build. Mater.* **2023**, *391*, 131845. [CrossRef]
30. Ranjbar, N.; Mehrali, M.; Behnia, A.; Javadi Pordsari, A.; Mehrali, M.; Alengaram, U.J.; Jumaat, M.Z. A Comprehensive Study of the Polypropylene Fiber Reinforced Fly Ash Based Geopolymer. *PLoS ONE* **2016**, *11*, e0147546. [CrossRef] [PubMed]